Month-Long 2D Cloud-Resolving Model Simulation and Resultant Statistics of Cloud Systems Over the ARM SGP

X. Wu
Department of Geological and Atmospheric Sciences
Iowa State University
Ames, Iowa

X.-Z. Liang
Illinois State Water Survey
University of Illinois
Urbana-Champaign, Illinois

Introduction

The cloud-resolving model (CRM) has recently emerged as a useful tool to develop improved representations of convections, clouds, and cloud-radiation interactions in general circulation models (GCMs). In particular, the fine spatial resolution allows the CRM to more realistically represent the detailed structure of cloud systems, including cloud geometric and radiative properties. The CRM simulations thus provide unique and comprehensive datasets, based on which more realistic GCM parameterization of sub-grid cloud-radiation interactions can be developed. To facilitate this, long-term CRM simulations are required to construct robust statistics of cloud structure and cloud-radiation interactions. While the evolving large-scale forcing from Global Atmospheric Research Program Atlantic Tropical Experiment (GATE) and Tropical Ocean Global Atmosphere-Coupled Ocean Atmosphere Response Experiment (TOGA-COARE) field experiments, allows the CRM to reproduce the long-term evolution of tropical cloud systems with a desirable degree of realism, the Atmospheric Radiation Measurement (ARM) intensive operational period (IOP) measurements provide a unique opportunity to apply the CRM for simulating mid-latitude continental cloud systems.

The CRM used in this study is based on the Clark-Hall model (Clark et al. 1996), which is a finite-difference formulation of the anelastic and nonhydrostatic equations. We improved the model physics to make the model applicable to cloud system studies, e.g., by adding an interactive cloud-radiation scheme based on the National Center for Atmospheric Research (NCAR) Community Climate Model Version 3 (CCM3; Kiehl et al. 1996), which calculates atmospheric radiative heating rates and surface radiation fluxes every 300 s. The cloud microphysics is parameterized using the Kessler (1969) bulk parameterization of the warm rain processes and a modified version of the Koenig and Murray (1976) ice parameterization (Wu et al. 1999). The subgrid-scale mixing is parameterized using the first-order eddy diffusion scheme of Smagorinsky (1963). Due to the lack of surface moisture measurement, the CRM is forced with evolving surface latent and sensible heat flux observed during the ARM 1997 IOP.

The two-dimensional (2D) domain is aligned east-west with 600 km long and 40 km deep. The model has a 3-km horizontal resolution and a stretched grid in the vertical (100 m at the surface, increasing to 1500 m at the model top). Periodic lateral boundary conditions are used to facilitate a mathematically consistent CRM framework (e.g., Grabowski et al. 1996). Free-slip bottom and top boundary conditions are applied together with a gravity wave absorber above the 16 km in the domain. The surface friction is calculated to model the momentum exchange between the air and ground. A 26-day (June 22-July 17) simulation during the ARM 1997 IOP is performed with a time step of 15 s. A random perturbation with the amplitude of 0.5 K is added to the temperature field below 3 km across the 2D domain.

The large-scale forcing was produced by the ARM using the constrained variational analysis (Zhang and Lin 1997). The version of the data used in this study was provided by Shaocheng Xie at LLNL, Livermore. Figures 1, 2, and 3 present the large-scale temperature, moisture, wind, surface sensible, and latent heat fluxes during the entire ARM 1997 IOP. A major feature needs to be mentioned is the passage of cold front during the July 3-4. There is strong moistening below 3 km in July 3 (Figure 1b), but there is no much temperature forcing (Figure 1a). The moisture is built up ahead of cold front. The strong cooling and moistening concur when the cold front pass through the Southern Great Plains (SGP) site in the early July 4 (Figures 1a and 1b). A strong upper level westerly jet is shown during July 2-6 in Figure 2a. The strong diurnal variation of surface heat fluxes is evident throughout the period in Figure 3.

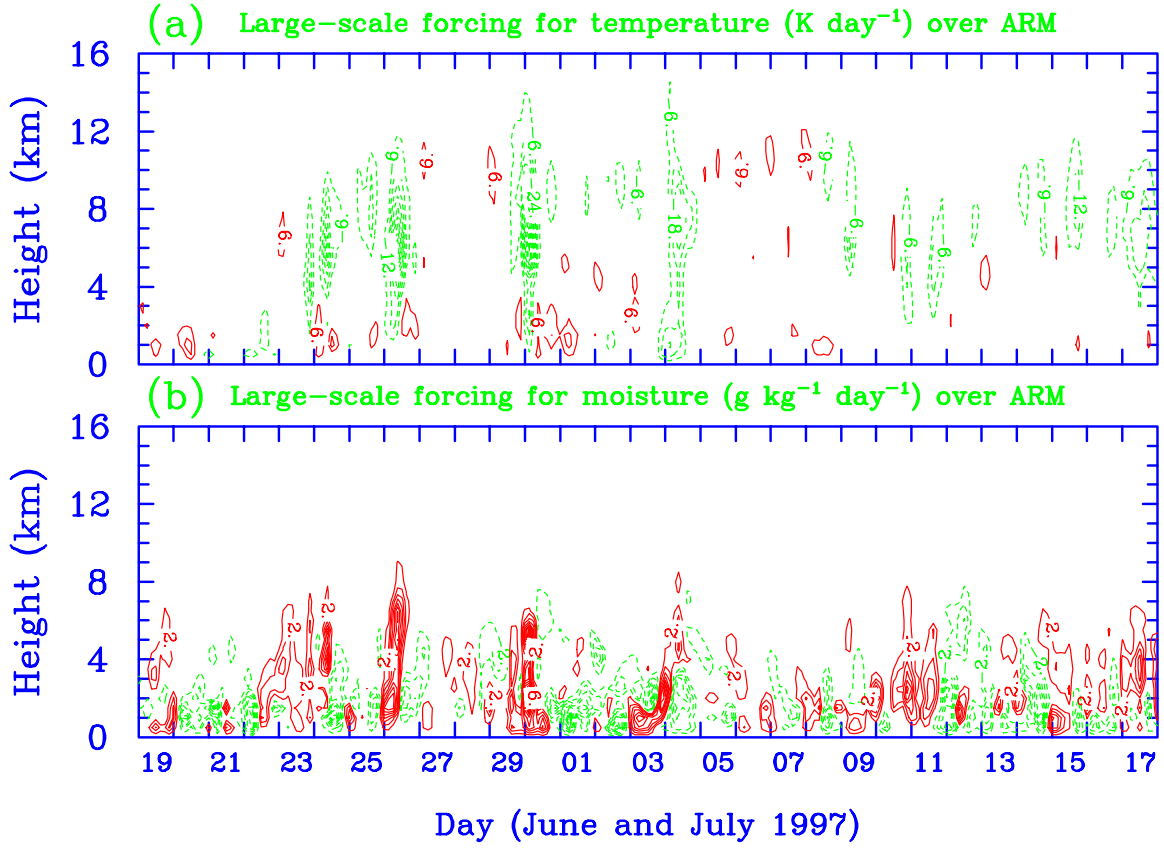

Figure 1. Large-scale forcing for (a) temperature and (b) moisture fields over the SGP during the ARM 1997 IOP.

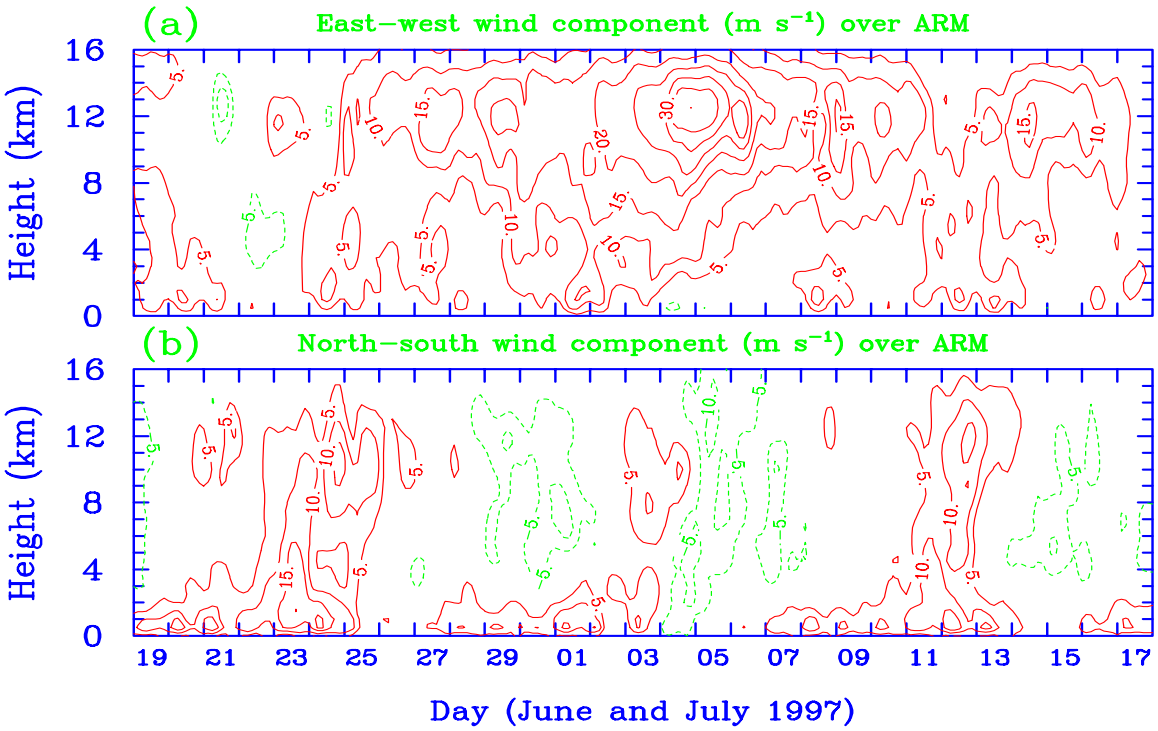

Figure 2. (a) Zonal and (b) meridional components of large-scale wind field over the SGP during the ARM 1997 IOP.

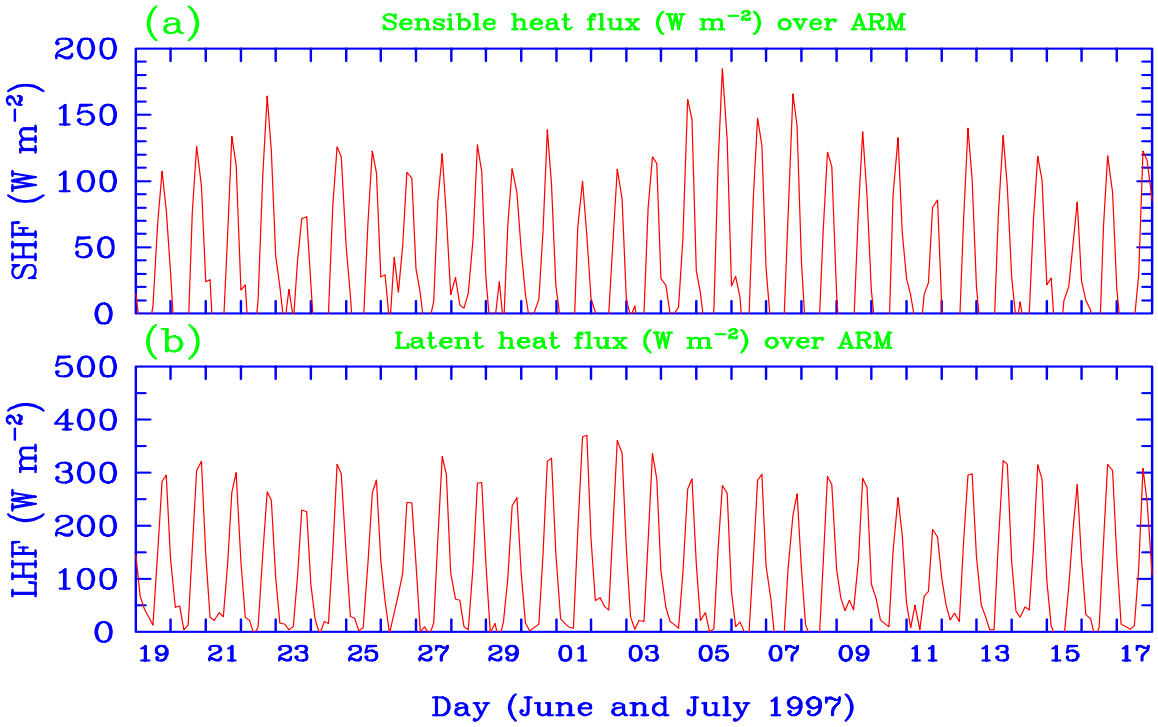

Figure 3. The surface (a) sensible and (b) latent heat fluxes over the SGP during the ARM 1997 IOP.

Simulated Cloud Systems and Evaluation Against ARM Observations

The CRM can be considered as a downscaling process, with which the high resolution cloud-scale properties can be reproduced by combining the large-scale forcing with the model physics. Figure 4 compares the CRM-produced and the observed precipitation over the 26-day period. The model result is averaged over the 600-km horizontal domain. The CRM successfully simulates the several precipitation events during the IOP. The temperature perturbation added below 3 km played an important role in the simulation of precipitation associated with the cold front in July 3-4. Without the perturbation, the moisture and energy are accumulated. When the cold front passed through the domain, convection exploded and produced unrealistically greater precipitation compared to the observation.

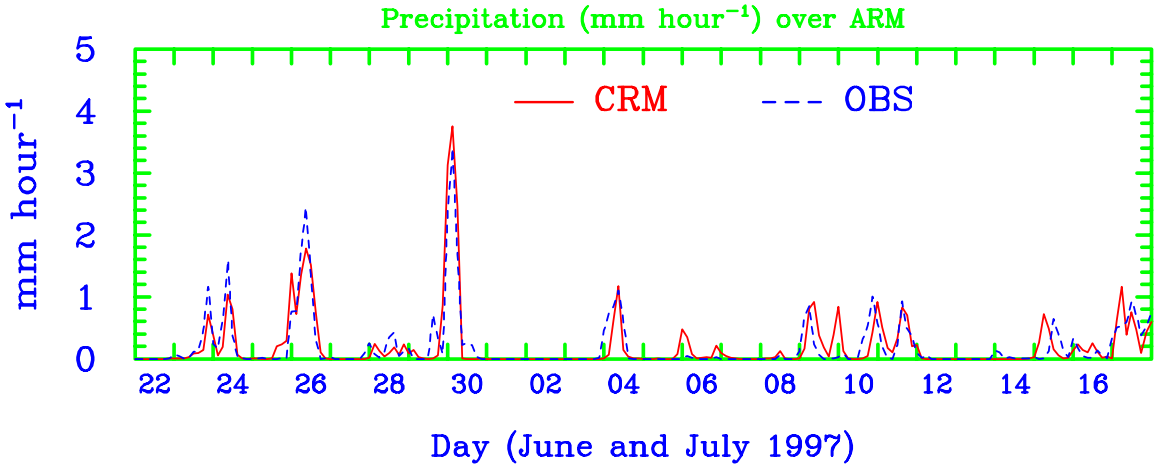

Figure 4. Three-hourly domain-averaged surface rainfall rates from the CRM (solid) and observation (dashed) over the SGP.

The cloud properties also compare favorably with the ARM measurements. The evolution of cloud liquid water is consistent with the observation (Figure 5a). Note that the observation is from the measurements at the four sounding stations within the SGP, but the model result represents the mean over the SGP domain. The CRM-produced cloud ice water is shown in Figure 5b, which can be evaluated when the observational estimate is available. The cloud ice water is generally larger than the cloud liquid water with the largest amount associated with convection on June 30 and July 4. The reliable cloud ice measurement is crucial for further improving the treatment of ice nucleation process and ice fall speed in the ice microphysical scheme used in the CRMs (e.g., Wu et al. 1999).

The intense radiation measurement from the ARM program provides important data to evaluate the performance of CRM. Table 1 lists the radiative fluxes at the top of the atmosphere (TOA) and the surface (SFC) averaged over the 26-day period. The observed surface shortwave radiative flux is estimated using Li's approach (Li et al. 1993). The TOA longwave and shortwave fluxes are obtained from Minnis's research group.

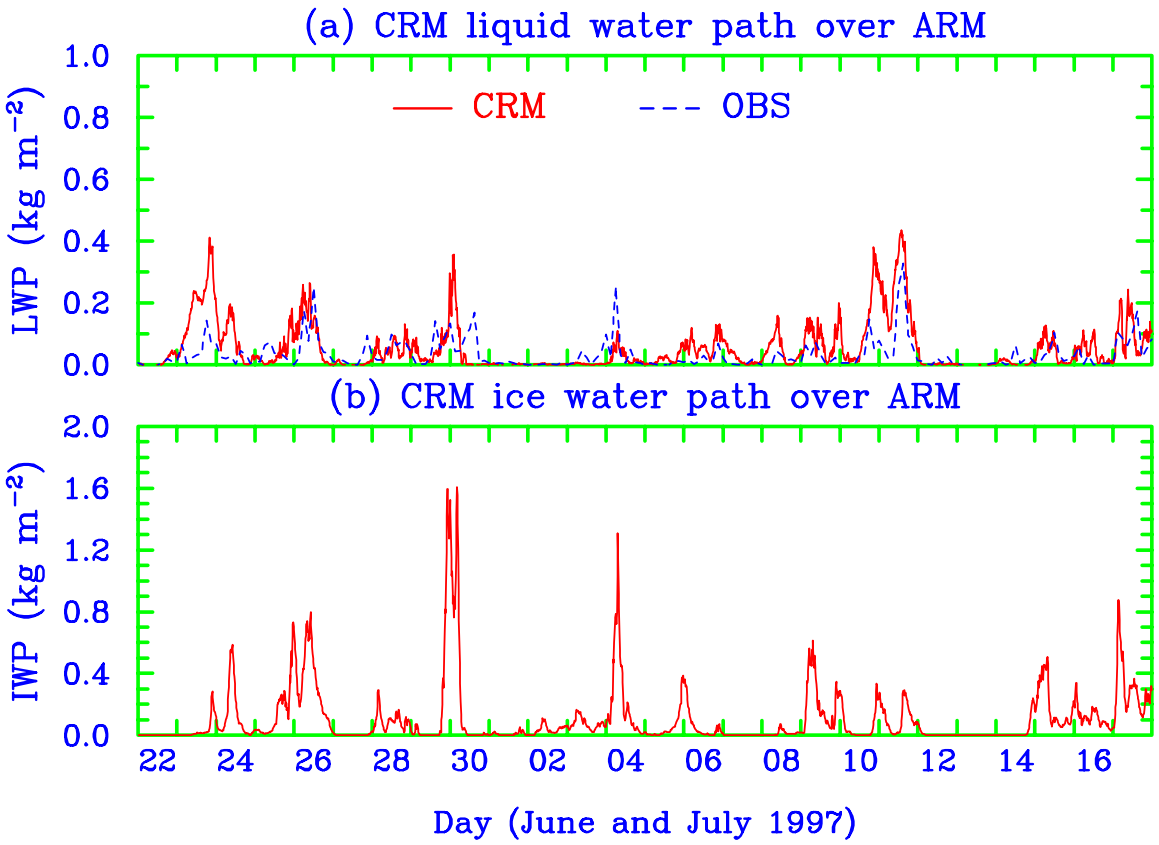

Figure 5. Evolution of (a) cloud liquid water and (b) cloud ice water from the CRM (solid) and observation (dashed). The model data is every 15 minutes, and the observational data is every 3 hours.

Table 1. 26-day mean TOA and SFC radiative fluxes from the CRM and observations.

Flux(Wm^{-2})	CRM	OBS
Q_{LW}(TOA)	-248.9	-259.1
Q_{SW}(TOA)	355.2	359.3
Q_{LW}(SFC)	-62.7	-62.6
Q_{SW}(SFC)	257.0	253.8

The longwave radiative flux at the surface is measured at the solar infrared stations (SIRS). The CRM result is averaged over the 600-km domain. It shows that the CRM- produced both longwave and shortwave radiative fluxes at TOA and SFC simultaneously agree with observational estimates within the measurement uncertainty. This result combined with our previous TOGA-COARE works (Wu and Moncrieff 2001) demonstrates that the cloud-radiation interaction is reasonably reproduced by the CRM over both land and ocean.

The 3-hourly ratio of downward all-sky over clear-sky shortwave fluxes at the surface from the CRM is plotted against the observational analysis from the Surface Cloud Grid Value Added Product (Long and Ackerman 2000) in Figure 6. Most points during the 26-day period fall within the observational uncertainty of 15%. The 26-day means (standard deviation) are 0.80 (0.16) and 0.82 (0.16) for the CRM and observation, respectively.

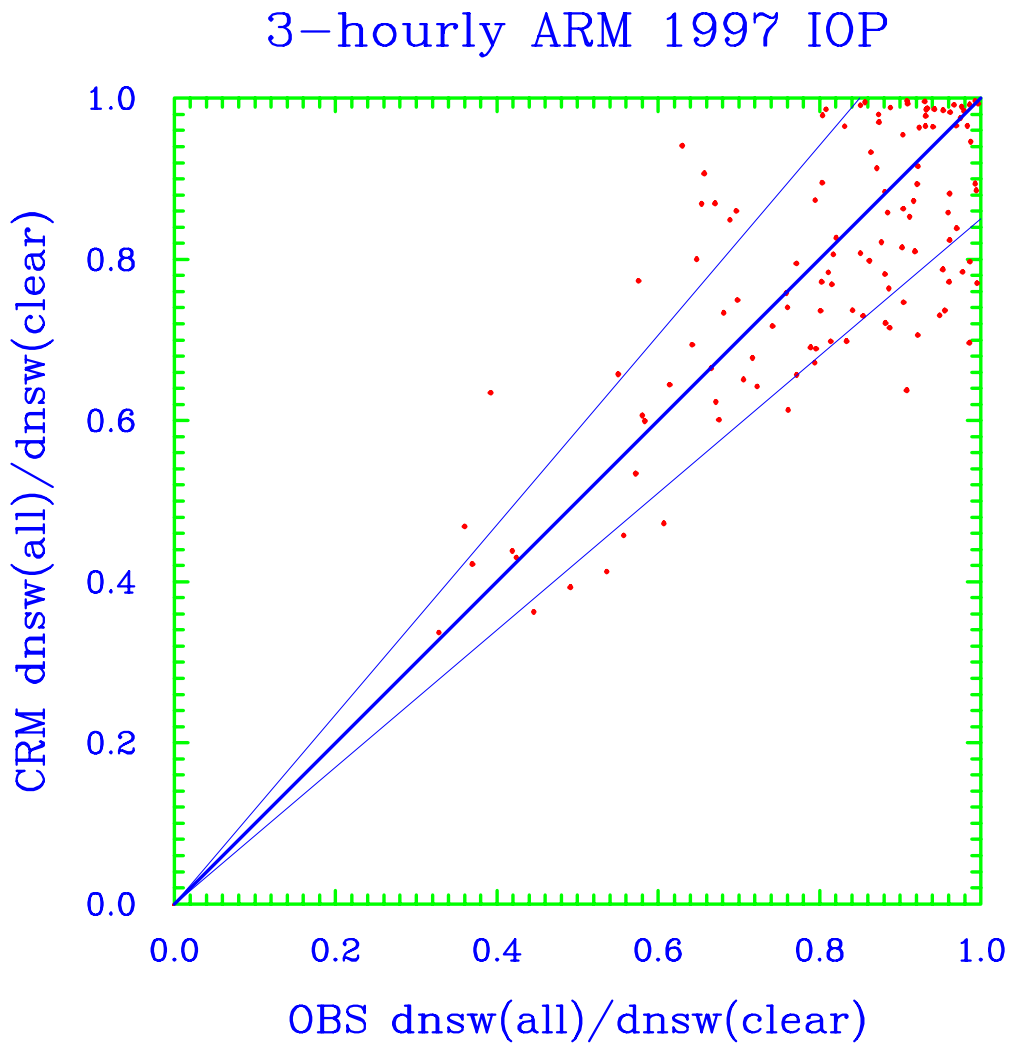

Figure 6. Ratio of downward all-sky over clear-sky shortwave fluxes at the surface from the CRM versus that from SfcCldGrid data.

Effects of Subgrid-Scale Variability

The successful downscale modeling of cloud and radiative properties allows the quantification of contributions of the subgrid-scale variability in the horizontal and vertical distribution of clouds and convection for the radiation calculation. Table 2 summarizes the two offline radiation calculations using the CRM-produced cloud-scale dataset. In the CRM simulation, the binary clouds (i.e., completely overcast or clear skies) are used for 200 columns. The radiative flux is calculated for each column using

the radiative transfer model, and the 200 values are then averaged to get the mean radiative flux. In the offline calculation M2, the cloud inhomogeneity is removed as follows. For each completely overcast column at a given level, the cloud properties are replaced by the domain-averaged value. The radiative flux is then calculated for each column and the mean flux is obtained by averaging all 200 columns. In the offline calculation M1, the mean cloud radiative properties and cloud fraction profiles are calculated from 200 columns first and the radiative flux is then computed using the way as in GCMs. In this calculation, the radiative transfer is computed once and the cloud vertical distribution has to be treated by the random cloud-overlap assumption.

Table 2. 26-day (June 22-July 17, 1997) mean TOA and SFC radiative fluxes from the CRM and offline radiation calculations (M2 and M1).

Flux (Wm^{-2})	CRM	M2 (CRM-M2)		M1 (M2-M1)	
Q_{LW}(TOA)	-248.9	-239.9	(-9.0)	-228.9	(-11)
Q_{LW}(SFC)	-62.7	-60.3	(-2.4)	-54.9	(-5.4)
Q_{SW}(TOA)	355.2	330.8	(24.4)	324.7	(6.1)
Q_{SW}(SFC)	257.0	231.0	(26.0)	225.4	(5.6)

The comparison between the CRM, M2, and M1 leads to the similar results obtained in our TOGA-COARE works (Wu and Moncrieff 2001). For the shortwave flux, the cloud horizontal inhomogeneity has a much larger impact on the flux than the vertical overlap assumption. For the longwave flux, both the cloud horizontal inhomogeneity and vertical overlap assumption are equally important.

The vertical profiles of shortwave, longwave, and total radiative heating and cooling are shown in Figure 7 for the CRM, M2, and M1. The use of homogeneous cloud properties (M2) produces systematically warmer radiative heating between 2 and 12 km, which results from the overwhelming longwave (shortwave) effect in the lower (upper) portion. As compared with the M2, the M1 produces further warming below 7 km while more cooling aloft. Note that the difference between the M1 and M2 is simply the cloud overlap assumptions (random versus realistic). Our result agrees with the finding of Liang and Wang (1997), where the mosaic approach closely resembles the M2 calculation. The difference between the CRM, M2, and M1 profiles further demonstrate the effects of subgrid-scale cloud variability, which will certainly affect GCM climate simulations (e.g., Liang and Wang 1997).

Statistics of Cloud Properties and the Mosaic Approach

The analysis of CRM-produced cloud-scale properties demonstrates the importance of subgrid cloud-radiation interactions. In order to include this aspect in the GCM radiation transfer parameterizations, the statistics of cloud geometric association and optical property inhomogeneity needs to be derived using the long-term CRM simulations. The CRM-based probability distribution functions (PDFs) will be incorporated into the mosaic approach (Liang and Wang 1997) for improving the parameterization of cloud-radiation interaction in GCMs. This can be considered as an upscaling process.

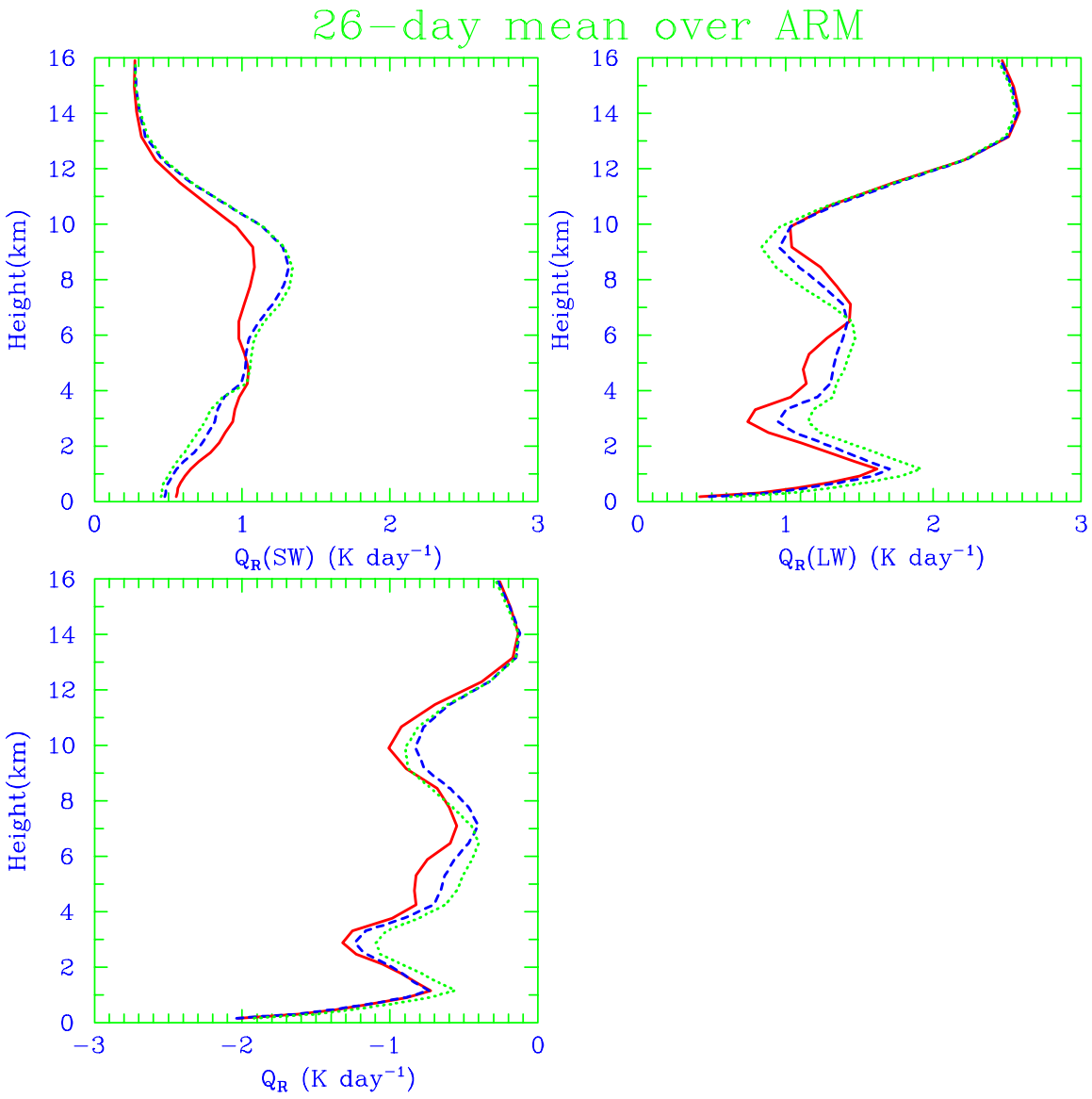

Figure 7. The 26-day mean profiles of (a) shortwave heating rates, (b) longwave heating rates, and (c) total radiative heating rates for the CRM (solid), M2 (dashed) and M1 (dotted).

The cloud frequency distributions are presented in Figure 8. All 15-minute samples at a 3-km horizontal resolution over the 600-km domain are used to identify all-layer clouds (no distinction on cloudy layer continuation), single-tower clouds (having a single unbroken segment in the entire vertical column), and two-layer clouds (two unbroken segments separated by 1 or more clear layers in the vertical column). Three major cloud types are evident: (1) shallow clouds with cloud base near 2.5 km; deep clouds with the base centered at 4 km and the top reaching 10 km or higher; (2) upper-level clouds with the base between 6-7 km; and (4) the middle clouds with the base at 4 km. These types are similar to the TOGA result (not shown). In addition, a distinct frequency center for the two-layer clouds occurs when the lower-layer cloud top between 5-6 km and the upper-layer cloud base at 7-8 km. This category seems different from the TOGA, where three preferred centers are identified. These cloud frequency

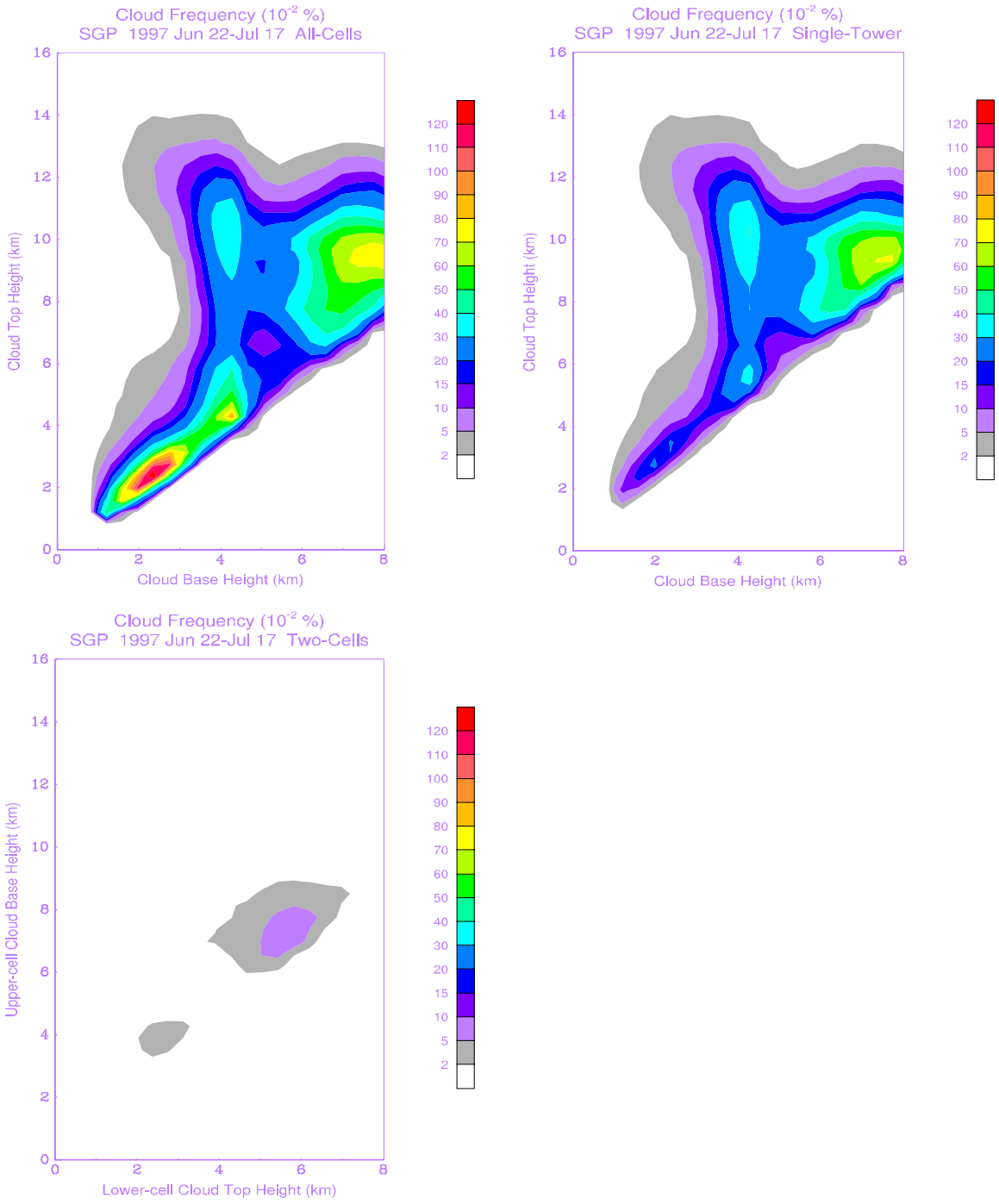

Figure 8. Cloud statistics simulated by the CRM at the SGP during June 22-July 17 for all-cell clouds (no distinction on cloudy layer continuation), single-tower clouds (having a single unbroken segment in the entire vertical column) and two-cell clouds (two unbroken segments separated by clear layers in the vertical column). The cloud frequency (10-2) is shown as a function of cloud base and top heights for all-layer and single-tower clouds, while that for two-layer clouds is depicted as lower-layer cloud top height (horizontal axis) and upper-layer cloud base height (vertical axis).

distributions and subsequent results of associated cloud property statistics will be useful to construct necessary PDFs to incorporate subgrid cloud-radiation interactions into GCM parameterizations, such as the mosaic approach (Liang and Wang 1997).

Acknowledgements

We thank the following Atmospheric Radiation Measurement Program scientists for providing the observational data in this study: Z. Li, M. Cribb and A. Trishchenko (surface shortwave flux data); C. N. Long (SfcCldGrid VAP data); P. Minnis and M. Khaiyer (GOES LBTM gridded dataset), M. Zhang, R. Cederwall, S. Xie, and J. Yio (observation and forcing data). This research is supported by the Office of Science (BER), U.S. Department of Energy, Grant No. DE-FG02-02ER63483.

Corresponding Author

Xiaoqing Wu, wuxq@iastate.edu, (515) 294-9872

References

Hall Cloud-Scale Model: Code Version G3CH01. NCAR Technical Note, NCAR/TN-426+STR. p. 137. (Available from NCAR Information Service, P.O. Box 3000, Boulder, CO 80307)

Grabowski, W. W., X. Wu, and M. W. Moncrieff, 1996: Cloud resolving modeling of tropical cloud systems during Phase III of GATE. Part I: Two-Dimensional Experiments. *J. Atmos. Sci*., **53**, 3684-3709.

Kessler, E., 1969: On the distribution and continuity of water substance in atmospheric circulations. *Meteor. Monogr*., **10**, No.32, p. 84.

Kiehl, J. T., J. J. Hack, G. B. Bonan, B. A. Boville, B. P. Briegleb, D. L. Williamson, and P. J. Rasch, 1996: Description of the NCAR Community Climate Model (CCM3). NCAR Tech. Note, NCAR/TN420+STR, p. 152. (Available from NCAR Information Service, P.O. Box 3000, Boulder, CO 80307.)

Koenig, L. R., and F. W. Murray, 1976: Ice-bearing cumulus clouds evolution: Numerical Simulation and General Comparison Against Observations. *J. Appl. Meteor*., **15**, 747-762.

Li, Z., H. G. Leighton, K. Masuda, and T. Takashima, 1993: Estimation of SW flux absorbed at the surface from TOA reflected flux. *J. Climate*, **6**, 317-330.

Liang, X.-Z., and W.-C. Wang, 1997: Cloud overlap effect on general circulation model climate simulations. *J. Geophys. Res.*, **102**, 11,039-11,047.

Long, C. N., and T. P. Ackerman, 2000: Identification of clear skies from broadband pyranometer measurements and calculation of downwelling shortwave cloud effects. *J. Geophy. Res*., **105**, 15,609-15,626.

Smagorinsky, J., 1963: General circulation experiments with the primitive equations. I. The Basic Experiment. *Mon. Wea. Rev*., **91**, 99-164.

Wu, X., and M. W. Moncrieff, 2001: Long-term behavior of cloud systems in TOGA COARE and their interactions with radiative and surface processes. Part III: Effects on the Energy Budget and SST. *J. Atmos. Sci*., **58**, 1155-1168.

Wu, X., W. D. Hall, W. W. Grabowski, M. W. Moncrieff, W. D. Collins, and J. T. Kiehl, 1999: Long-term behavior of cloud systems in TOGA COARE and their interactions with radiative and surface processes. Part II: Effects of Ice Microphysics on Cloud-Radiation Interaction. *J. Atmos. Sci*., **56**, 3177-3195.

Zhang, M. H., and J. L. Lin, 1997: Constrained variational analysis of sounding data based on column-integrated conservations of mass, heat, moisture, and momentum: Approach and Application to ARM Measurements. *J. Atmos. Sci*., **54**, 1503-1524